# Lifetime measurements in $^{102}$Pd: Searching for empirical proof of the E(5) critical-point symmetry in nuclear structure

T. Konstantinopoulos,[*] S. F. Ashley,[†] M. Axiotis, A. Spyrou,[‡] and S. Harissopulos[§]
*TANDEM Accelerator Laboratory, Institute of Nuclear and Particle Physics, NCSR "Demokritos," 15310 Aghia Paraskevi, Athens, Greece*

A. Dewald, J. Litzinger, O. Möller,[‖] and C. Müller-Gatterman
*Institut für Kernphysik, Universität zu Köln, Zülpicherstr. 77, 50937 Köln, Germany*

P. Petkov[††]
*INRNE, Bulgarian Academy of Sciences, 1784 Sofia, Bulgaria*

D. R. Napoli, N. Marginean,[¶] and G. de Angelis
*INFN—Laboratori Nazionali di Legnaro, Viale dell'Università 2, 35020 Legnaro, Italy*

C. A. Ur,[¶] D. Bazzacco, E. Farnea,[**] and S. M. Lenzi
*Dipartimento di Fisica dell' Università and INFN, Sezione di Padova, via Marzolo 8, 35131 Padova, Italy*

R. Vlastou
*National Technical University of Athens—NTUA, Zographou Campus, 15780 Athens, Greece*

D. Balabanski[††]
*Dipartimento di Fisica, Universita di Camerino and INFN, Sezione di Perugia, 62032 Camerino, Italy*
(Received 2 February 2013; revised manuscript received 28 October 2015; published 27 January 2016)

Lifetimes of yrast and nonyrast states of $^{102}$Pd populated via the $^{92}$Zr($^{13}$C, $3n$) reaction are measured by means of the recoil distance Doppler-shift technique with a Cologne plunger coupled to a GASP spectrometer. The event-by-event data accumulated at 24 plunger distances in the range of 0.1 $\mu$m to 9 mm are analyzed using the differential decay curve method. The resulting $B(E2)$ values of the $\gamma$ transitions depopulating yrast-band members up to the $I^{\pi} = 8^{+}$ state are found to deviate significantly from the corresponding predictions of the E(5) critical-point symmetry.

DOI: 10.1103/PhysRevC.93.014320

## I. INTRODUCTION

Fifteen years ago, a new class of dynamical symmetries, the so-called E(5) and X(5) critical-point symmetries, was introduced by Iachello [1,2] in nuclear structure. These symmetries are used to describe spectra of nuclei that are located at or around the critical point of shape-phase transitions. As such, X(5) refers to a nucleus at the "critical point" where its shape changes from a prolate-deformed symmetric rotor [3] to a spherical harmonic vibrator [4]. Similarly, E(5) describes the shape change of a spherical harmonic vibrator to that of a "$\gamma$-soft" rotor [5]. In the infinite boson limit of the elementary formulation of the so-called interacting boson approximation (IBA) model, i.e., IBA-1 [6], these three "geometrical" pictures of nuclear collective excitations correspond to the well-known SU(3), U(5), and O(6) limits. The IBA has provided, for more than 30 years, a sound theoretical ground for the description of the structure at low excitation energies of collective nuclei. This description is based on the dynamical symmetries of the U(6) Lie algebra from which three subalgebras corresponding to the SU(3), U(5), and O(6) limits are obtained.

As in the case of the three dynamical symmetries of IBA-1, both the E(5) and the X(5) critical-point symmetries provide parameter-free predictions (except for scale) for energies and reduced transition probabilities. In addition, the E(5) and X(5) symmetries also provide parameter-free predictions for the ratios of excitation energies. Given these, the search for empirical proofs of the E(5) and X(5) shape-phase transitions has become an attractive task for experimentalists over the past decade. To date, the X(5) symmetry is well established

[*]Present address: CSNSM, IN2P3-CNRS, and Université Paris-Sud, F-91405 Orsay, France.
[†]Present address: Department of Engineering and Innovation, The Open University, Milton Keynes MK7 6AA, UK.
[‡]Present address: NCSL, Michigan State University, East Lansing, Michigan 48824, USA.
[§]sharisop@inp.demokritos.gr
[‖]Present address: Institut für Kernphysik, Technische Universität Darmstadt, Schlossgartenstr. 9, 64289 Darmstadt, Germany.
[¶]Present address: Horia Hulubei National Institute of Physics and Nuclear Engineering—IFIN HH, P.O. Box MG-6, Bucharest-Magurele, Romania.
[**]Deceased.
[††]Present address: ELI-NP, Horia Hulubei National Institute of Physics and Nuclear Engineering, 077125 Magurele, Romania.

 

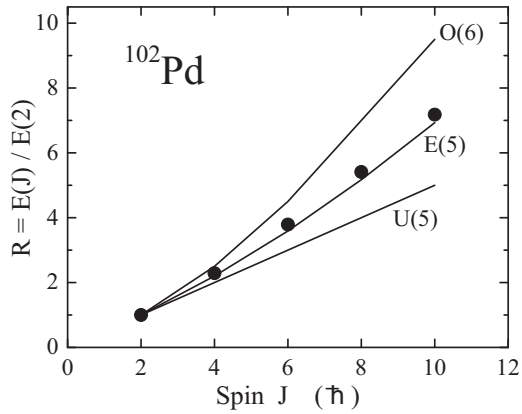


FIG. 1. Experimental energy ratios $R = E(J)/E(2)$ (filled circles) of the ground band members of $^{102}$Pd and corresponding predictions (solid lines) of the E(5) symmetry and the O(6) and U(5) limits of the IBA for an infinite number of bosons.

and the $N = 90$ $^{152}$Sm [7], $^{150}$Nd [8], and $^{154}$Gd [9] isotones, as well as the Os nuclei with $A \approx 180$ [10], are taken as the best X(5)-symmetry realizations in nuclear structure. These nuclei exhibit X(5) features not only in terms of their excitation spectra but also in the $B(E2)$ strengths of $\gamma$ transitions depopulating the lowest-lying states of their ground as well as the $\beta$ and $\gamma$ (the so-called S2, S3, etc.) side bands.

The first empirical proof of the E(5) symmetry was reported in $^{134}$Ba [11] simultaneously with the letter by Iachello introducing E(5) [1]. In the former letter [11], it was additionally mentioned that some Pd isotopes could be good E(5) candidates. Later, Zamfir *et al.* [12] investigated the excited states of $^{102}$Pd populated via the $\epsilon/\beta^+$ decay of $^{102}$Ag and found that the level scheme of $^{102}$Pd is in good overall agreement with the E(5) predictions. In addition, Clark *et al.* [13] examined key properties of even-even nuclei with $A > 60$ and proposed six nuclei including $^{102}$Pd as the most promising cases of nuclei at the E(5) critical point. Indeed, as shown in Fig. 1, the energy ratios of the ground band members of $^{102}$Pd are in excellent agreement with those predicted by the E(5) critical-point symmetry; however, no information on the $B(E2)$ values of states lying higher than the $4_1^+$ level was known at the time that Refs. [12] and [13] were published. These findings motivated us to measure the lifetimes of excited states in the ground band of $^{102}$Pd with the aim of deriving the corresponding missing absolute transition probabilities which allow the performance of a very sensitive test of the suggested E(5) character of this nucleus. The present paper reports on the results of these measurements.

It is worth noting that during the time of the preparation of the current paper, another article on $^{102}$Pd was published by Ayangeakaa *et al.* [14], where the lifetimes of yrast states $\geqslant 6^+$ were measured using the Doppler-shift attenuation method. A comparison of these data with our results is reported in Sec. III A.

## II. EXPERIMENTAL SETUP AND PROCEDURES

The lifetime measurements of the present work were performed at the Laboratori Nazionali di Legnaro, Italy. The recoil distance Doppler-shift method [15,16] was applied using a Cologne plunger device, which was coupled to a GASP spectrometer [17]. TheGASP comprises 40 large-volume Compton-suppressed high-purity Ge detectors and an inner ball of 80 BGO elements in the so-called "configuration I.' The BGO elements can be removed ('configuration II") so that the distance of the high-purity Ge detectors from the target is decreased from 27 to ≈20 cm, resulting in this way in an increase in the total detection efficiency, which is primarily required for lifetime measurements. That latter configuration is the one used in the present work. The GASP's high-purity Ge detectors are grouped in seven rings around the target, each corresponding to a well-defined polar angle of 34.5°, 59.4°, 72°, 90°, 108°, 120.6°, and 145.4° with respect to the beam axis. In the following, these rings are coined rings 0, 1, 2, 3, 4, 5, and 6, respectively.

Excited states in $^{102}$Pd were populated using the $^{92}$Zr($^{13}$C,$3n$)$^{102}$Pd fusion-evaporation reaction. The energy of the $^{13}$C beam provided by the XTU Tandem Van de Graaff accelerator at Laboratori Nazionali di Legnaro was 48 MeV. Its intensity ranged from ≈3 to ≈5 pnA over 160 h of operation. The target foil was ≈1.1 mg/cm$^2$ thick and enriched in $^{92}$Zr to 95.13%. The recoiling $^{102}$Pd nuclei were stopped in a gold foil (stopper) 4 mg/cm$^2$ thick. The mean recoil velocity of the evaporation residues was ∼0.80(3)% of the speed of light $c$.

Event-by-event data were recorded at 24 target-to-stopper distances, referred to hereafter as "plunger" distances, ranging from 0.1 $\mu$m to 9 mm. The distances were maintained by means of a piezoelectric device equipped with a feedback loop to check the stability of the plunger distances and regulate possible variations over time. For a valid event to be recorded for off-line analysis, coincident $\gamma$ rays had to be detected by at least two high-purity Ge detectors. Valid events were sorted into $\gamma$-ray energy vs $\gamma$-ray energy matrices for all ring combinations and for each individual distance. In total, $7 \times 7 \times 24 = 1176$ matrices were generated, each consisting of $4096 \times 4096$ Analog-to-Digital-Converter channels. A typical total projection spectrum of ring 6 at 145.4° produced by gating on all $\gamma$ rays detected in ring 0 at 34.5° at a plunger distance of 7.9 $\mu$m is shown in Fig. 2.

## III. DATA ANALYSIS AND RESULTS

The matrices that resulted from the sorting of the event-by-event data acquired by rings 0, 1, 5, and 6 were used to produce suitable $\gamma$-gated spectra (cuts). These were used to apply the differential decay curve method (DDCM) that has been proved to be a very reliable method of analysis of Doppler-shift-based measurements in $\gamma$-$\gamma$ coincidence as well as in $\gamma$-singles mode. As the DDCM is discussed in detail elsewhere [18,19], only the pertinent aspects of this method are described.

According to the DDCM in $\gamma$-$\gamma$-coincidence mode, the mean lifetime $\tau$ of the level of interest $L$ that is depopulated via transition $A$ can be determined at every plunger distance $x$ by gating either "indirectly" or "directly." In the latter case, a gate is set on the Doppler-shifted component of a transition, say $B$, that directly populates the level $L$. In this case, the mean

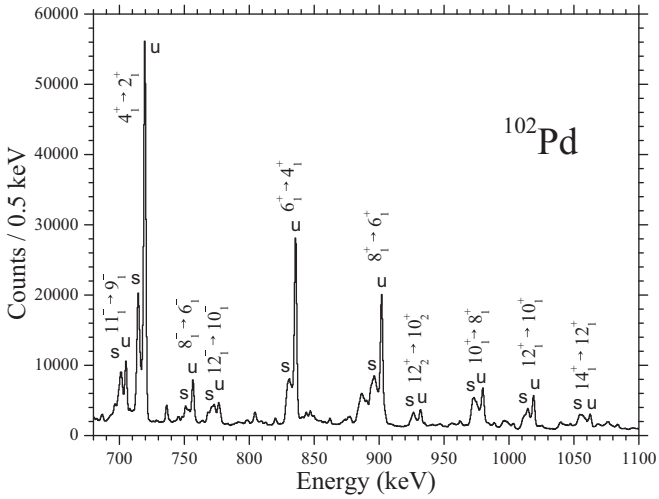


FIG. 2. Part of the projection of ring 6 (145.4°) generated by gating on all $\gamma$ rays detected by ring 0 (34.5°) at a distance of 29 $\mu$m. Doppler-unshifted components ("stop" peaks) of the strongest $\gamma$ transitions are labeled "u", whereas Doppler-shifted ones ("flight" peaks) are labeled "s".

lifetime $\tau_L$ is determined using

$$\tau_L(x) = \frac{I_u^A}{v \cdot \frac{d}{dx} I_s^A}, \tag{1}$$

where $v$ denotes the recoil velocity and the subscripts $s$ and $u$ refer to the Doppler-shifted ("flight" peak) and unshifted ("stop" peak) components, respectively, of the normalized intensities $I$ of the depopulating transition $A$.

In the case of indirect gating, the gate is set on a transition, say $C$, that depopulates a higher-lying state and feeds the level of interest, $L$, via intermediate transitions the last of which is the transition $B$, which directly feeds level $L$. Then $\tau_L$ is derived using

$$\tau_L(x) = \frac{I_u^A - \alpha \cdot I_u^B}{v \cdot \frac{dI_s^A}{dx}}, \tag{2}$$

with

$$\alpha = \frac{I_u^A + I_s^A}{I_u^B + I_s^B}. \tag{3}$$

By fitting the intensities of the shifted components with second-order polynomials, as described in [18], and the derivative of these polynomials to the stopped components, one obtains two curves for the Doppler-shifted and unshifted components, which are used to extract the lifetime at each target-to-stopper distance. These curves are called coincidence decay curves and are determined by the number of coincidences of the Doppler-shifted $\gamma$ rays of the gated feeding transition with the Doppler-unshifted or -shifted $\gamma$ rays of the depopulating transition. The individually determined lifetimes and their associated errors are then plotted on a so-called $\tau$ plot versus the target-to-stopper distance, $x$. The data points of a $\tau$ plot are expected to "statistically" lie on a straight line provided that unknown systematic errors are eliminated (see [18]).

In this work, Eqs. (1)–(3) were fitted to the data using the code NAPATAU [20]. The intensities $I$, which were derived from the spectra using the analysis program TV [21], were normalized as follows: A gate was set on the shifted and the unshifted components of a strong uncontaminated $\gamma$ transition in the ground band of $^{102}$Pd, such as the $6_1^+ \rightarrow 4_1^+$, and the intensities of the stop and flight peaks of certain $\gamma$ rays in the resulting spectra were summed. The summed intensities were then normalized to the sum obtained at the plunger distance of 4 $\mu$m, where spectra with the most statistics were taken. This procedure was repeated by gating on a number of strong transitions in the ground band, with the exception of the $2_1^+ \rightarrow 0_1^+$ $\gamma$ ray, to avoid possible uncertainties due to deorientation effects (see, e.g., [22]). The different normalization factors extracted using different gating transitions as described above were found to be consistent. Normalization factors were also extracted from the total integrals of projection spectra. These factors were found to agree very well with those obtained by the former gating procedure at plunger distances up to 240 $\mu$m. At larger distances deviations were observed, possibly due to solid angle effects. It is worth noting, however, that our results are not influenced by these deviations since the data points determined at plunger distances larger than 240 $\mu$m were not used in our data analysis. Data taken at longer distances were aimed at investigating possible long-lived feeding into the states of interest.

In our data analysis, the gating regions used were checked for possible contaminations in both the stop and the flight peaks arising from reaction channels other than the $3n$. Also, in order to ensure that the gating region set on a flight peak does not include any contaminant $\gamma$ rays from the tail of the corresponding stop peak, up to five gate widths were placed on each transition as shown in Fig. 3 and the following results were checked for systematic deviations in the measured lifetime. In the instance where systematic deviations were observed, the particular gating combination was not included in the final analysis.

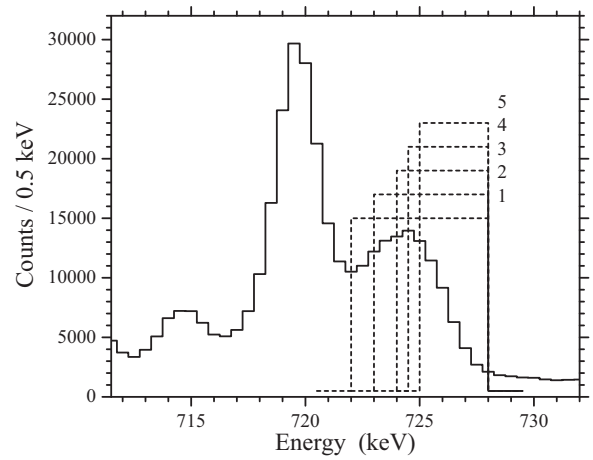


FIG. 3. Five gates with different widths set on the Doppler-shifted component of the $4_1^+ \rightarrow 2_1^+$ $\gamma$ transition to check for possible gate-width dependence of the mean lifetime of the $2_1^+$ state. Similarly, gates of different widths were set in all flight peaks used in the present work to apply the DDCM.

It must be noted also that the gating region chosen for each of the determined lifetimes covers a part of the shifted component of the feeder. Events in the more shifted part of the peak correspond to faster recoils, whereas the $\gamma$ rays emitted by the slower recoils appear less shifted. As a result, different gating regions correspond to different average velocities of the selected recoils. Therefore, the velocity was determined independently for each gate from the observed Doppler shift in the resulting cut spectrum.

Every mean lifetime reported in this work was determined by more than one different set of gates as well as more than one ring combination. In the following, when we refer to ring combinations, we use the notation "A_B," where B is the ring where the gate is set and A is the projection ring. Furthermore, when the ring combination "A_B,C" is mentioned, it means that the projections of gates (hereafter called "cuts") set on B and C were summed. Finally, when more than two cuts are added, in order to avoid confusing notation, the resulting cut is denoted "A_s," where s stands for sum.

In all cases, gates were set on transitions indirectly feeding the state, and with the exception of the analysis of the $4_1^+$ state, gates were also set on transitions directly feeding the state of interest. This not only ensures a transparent application of the DDCM but also eliminates uncertainties due to the deorientation effect [23]. Since no systematic deviation appeared for the levels analyzed when using direct or indirect gates, it was concluded that the deorientation effect was negligible, if existent.

### A. Yrast band lifetimes

In the following paragraphs, we give details of the analysis for each of the yrast band members for which a mean lifetime is reported. By employing the gating procedure described in the previous paragraphs, clean gated projection spectra were acquired, an example of which is shown in Fig. 4 for the $2_1^+ \rightarrow 0_1^+$ transition. As shown in this figure, the centroids of the stopped and flight components are well separated. Thus, the intensities of these components could be easily determined by two Gaussian peaks. Figure 5 shows typical coincidence decay curves and $\tau$ plots for the transitions depopulating the $2_1^+$, $4_1^+$, $6_1^+$, and $8_1^+$ states. The points in the $\tau$ plot correspond to the individual lifetime values deduced from the fit at each distance. The solid line in each $\tau$ plot represents the weighted mean value of those lifetimes and the dashed lines show the corresponding statistical error. By performing this procedure for different gates and various ring combinations, a number of separate lifetimes and their associated statistical errors were obtained. Details regarding the gates and ring combinations used and the lifetimes obtained are presented in the following paragraphs. Each separate lifetime deduced in this analysis is shown in Fig. 6 with its corresponding statistical error. Within this figure, the weighted mean of all these separate lifetimes is represented by a solid line. In order to account for any possible systematic error, the average weighted variance was taken as the total uncertainty of the final lifetime value and this error is depicted by the dashed lines. Table I lists the weighted mean lifetimes and associated errors for the $2_1^+$ to $8_1^+$ yrast band states and their corresponding $B(E2)$ values.

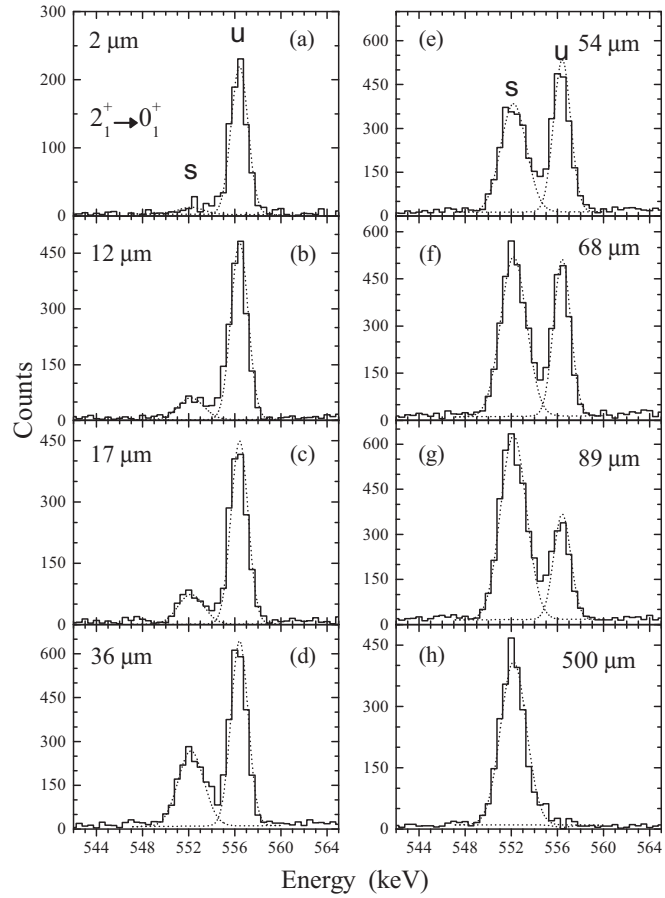


FIG. 4. Doppler-shifted (s) and unshifted (u) components of the $2_1^+ \rightarrow 0_1^+$ transition ($E_\gamma = 556$ keV) as projected in ring 6 when the gate is placed on the flight peak of the $4_1^+ \rightarrow 2_1^+$ transition in ring 0. Target-to-stopper distances of (a) 2 $\mu$m, (b) 12 $\mu$m, (c) 17 $\mu$m, (d) 36 $\mu$m, (e) 54 $\mu$m, (f) 68 $\mu$m, (g) 89 $\mu$m, and (h) 500 $\mu$m are displayed, in which the evolution from a completely stopped to a fully shifted peak is illustrated. Dashed curves indicate the fitting of the peaks from which the intensities $I$ entering Eq. [3] were derived.

#### 1. $I^\pi = 2_1^+$ state at $E_x = 556$ keV

Lifetimes for the $2_1^+$ state were determined by one set of direct gates and two sets of indirect gates. The direct gate was placed on the Doppler-shifted component of the 719-keV, $4_1^+ \rightarrow 2_1^+$ transition in rings 0 and 1. Due to contamination from the stopped component of the 715-keV, $9_1^- \rightarrow 8_1^+$ transition, the detector rings located at backward angles (i.e., rings 5 and 6) were not used. For the direct gate on the 719-keV transition, mean lifetimes of 17.5(2) and 18.2(2) ps were determined for the 6_0 and 6_1 ring combinations, respectively. The coincidence decay curves and corresponding $\tau$ plot for the 6_0 combination are shown in Figs. 5(a) and 5(b). One set of indirect gates was placed on the Doppler-shifted components of the 980-keV, $10_1^+ \rightarrow 8_1^+$ transition. Due to contaminations on both sides of the 980-keV photopeak, namely, at 970 and 987 keV, it was necessary to use narrow gates (~2 keV wide) on this transition. Since the flight component of the 980-keV $\gamma$ ray is less shifted in rings 1 and 5 (due to their smaller angles), we obtained

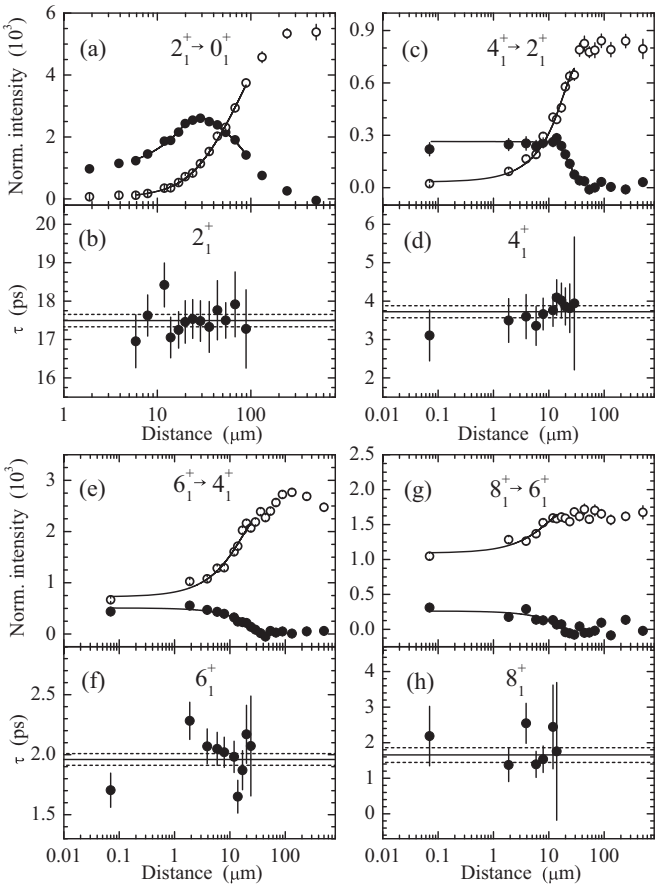


FIG. 5. Typical coincidence decay curves and $\tau$ plots for the $2_1^+$ to $8_1^+$ yrast band members. (a, c, e, g) The normalized intensities of the shifted (open circles) and unshifted (filled circles) components of the depopulating transition are shown with the corresponding fits from NAPATAU (solid lines). (b, d, f, h) The associated $\tau$ plots. Statistical errors are shown by dashed lines.

more statistics when gating in those rings and therefore they were used for gating instead of rings 0 and 6. For these indirect gates, lifetimes of 17.9(4), 17.6(4), 17.2(4), and 18.0(4) ps were determined for the 0_1, 0_5, 6_1, and 6_5 ring combinations, respectively. Another set of gates was placed on the Doppler-shifted components of the 1062-keV, $12_1^+ \rightarrow 10_1^+$ transition in rings 5 and 6. For this particular transition, rings 0 and 1 were not used for gating in the whole analysis due to contamination observed in the total-projection spectrum around 1070–1080 keV. For these indirect gates on the 1062-keV transition, 17.1(9), 16.1(8), and 17.3(7) ps were deduced for the 0_5, 6_5, and 6_6 ring combinations, respectively. The weighted mean of these nine lifetimes for the $2_1^+$ state is 17.7(4) ps, as shown in Fig. 6.

### 2. $I^\pi = 4_1^+$ state at $E_x = 1276$ keV

Lifetimes for the $4_1^+$ state were determined by two sets of indirect gates. No direct gate on the 835-keV, $6_1^+ \rightarrow 4_1^+$ transition was used due to an observed Doppler-shifted component of the 715-keV, $9_1^- \rightarrow 8_1^+$ transition in the gated spectra which overlapped with the 719-keV transition of interest. One set of

TABLE I. Mean lifetimes (third column) determined in the present work for the $2_1^+$ to $8_1^+$ yrast band members, as well as various negative-parity sideband levels, are listed. The spin and parity of these excited states and their corresponding excitation energies are listed in the first and second columns. The depopulating transitions and their $\gamma$-ray energies are given in the fourth and fifth columns, respectively. The deduced $B(E2)$ values (in Weisskopf units) are presented in the last column.

| $I_i^\pi$ | $E_x$ (keV) | $\tau$ (ps) | $I_i^\pi \rightarrow I_f^\pi$ | $E_\gamma$ (keV) | $B(E2)$ (W.u.) |
|---|---|---|---|---|---|
| $2_1^+$ | 556.4 | 17.7(4) | $2_1^+ \rightarrow 0_1^+$ | 556.4 | 30.4(7) |
| $4_1^+$ | 1275.9 | 3.7(3) | $4_1^+ \rightarrow 2_1^+$ | 719.4 | 40.3(29) |
| $6_1^+$ | 2111.4 | 2.0(1) | $6_1^+ \rightarrow 4_1^+$ | 835.5 | 35.5(17) |
| $8_1^+$ | 3013.1 | 1.9(2) | $8_1^+ \rightarrow 6_1^+$ | 901.7 | 24.9(29) |
| $8_1^-$ | 3670.6 | 11.9(3) | $8_1^- \rightarrow 6_1^-$ | 756.5 | 7.7(7) |
| $9_1^-$ | 3727.8 | 27.1(8) | $9_1^- \rightarrow 7_1^-$ | 539.7 | 4.6(12) |
| $10_1^-$ | 4317.8 | 6.5(6) | $10_1^- \rightarrow 8_1^-$ | 647.2 | 24.3(32) |

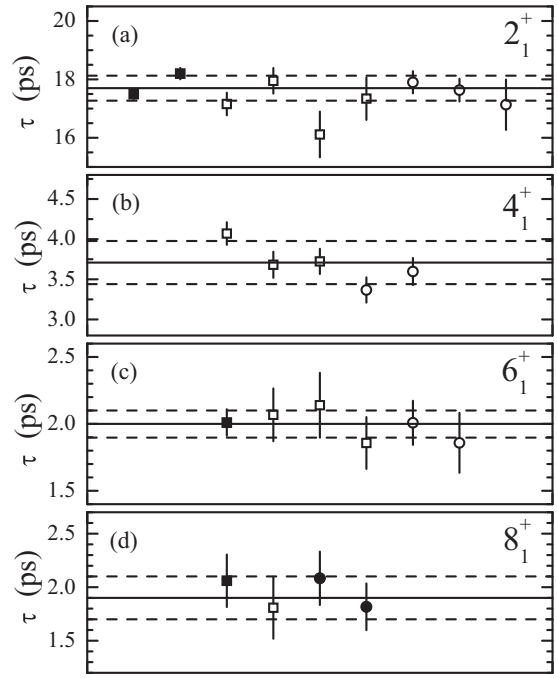


FIG. 6. Compilation of the weighted mean lifetimes of the yrast members (a) $2_1^+$, (b) $4_1^+$, (c) $6_1^+$, and (d) $8_1^+$ deduced in this work and their associated weighted errors. Filled symbols correspond to cases where direct gating was used, whereas open symbols correspond to indirect gating. Squares denote that the gated projection of ring 6 was used in that particular analysis. Circles denote that the gated projection of ring 0 was used instead. Each individual lifetime presented contains the statistical error from NAPATAU. To account for any possible systematic errors, the weighted average variance of the determined lifetimes was taken as the total uncertainty (see text). The weighted mean values (solid lines) as well as the errors in the weighted mean values (dashed lines) correspond to the values listed in Table I. Values shown for the $6_1^+$ and $8_1^+$ levels have the Doppler-shift attenuation correction incorporated.

indirect gates was placed on the Doppler-shifted components of the 980-keV, $10_1^+ \rightarrow 8_1^+$ transition in rings 1 and 5. For these indirect gates, lifetimes of 3.37(16), 3.60(17), 3.68(16), and 3.72(16) ps were observed for the 0_1, 0_5, 6_1, and 6_5 ring combinations, respectively. The resultant coincidence decay curves and $\tau$ plot for the 6_5 combination is shown in Figs. 5(c) and 5(d). The indirect gates were placed on the Doppler-shifted component of the 1062-keV, $12_1^+ \rightarrow 10_1^+$ transition in rings 5 and 6. It should be noted that, due to lack of statistics, cuts on the detectors located in rings 5 and 6 were summed for each projection ring. For these indirect gates on the 1062-keV transition, a lifetime of 4.07(14) ps was observed for the 0_5,6 ring combination. The weighted mean of these five lifetimes for the $4^+$ state is 3.71(27) ps, as shown in Fig. 6.

#### 3. $I^\pi = 6_1^+$ state at $E_x = 2111$ keV

Lifetimes for the $6_1^+$ state were determined by one set of direct gates and two sets of indirect gates. A direct gate was placed on the Doppler-shifted component of the 901-keV, $8_1^+ \rightarrow 6_1^+$ transition in ring 0. For this direct gate, a lifetime of 1.96(5) ps was deduced from the 6_0 ring combination. The coincidence decay curves and $\tau$ plot for this transition are shown in Figs. 5(e) and 5(f). Indirect gates were placed on the Doppler-shifted components of the 980-keV, $10_1^+ \rightarrow 8_1^+$ transition in rings 1 and 5. For these indirect gates, lifetimes of 1.96(14), 1.81(20), 2.02(17), and 2.09(22) ps were observed for the 0_1, 0_5, 6_1, and 6_5 ring combinations, respectively. Indirect gates were also placed on the Doppler-shifted component of the 1062-keV, $12_1^+ \rightarrow 10_1^+$ transition in rings 5 and 6. Similarly to the $4_1^+$ analysis, due to lack of statistics, cuts on the detectors located in rings 5 and 6 were summed for each projection ring. For these indirect gates, a lifetime of 1.81(19) ps was observed for the 6_5,6 ring combination. The weighted mean value of these six lifetimes for the $6_1^+$ state is 1.95(6) ps.

An additional correction was taken into account for the case of the $6_1^+$ level as well as for the $8_1^+$ level. This is due to the fact that in the solid material of the stopper the recoil does not come immediately at rest but in a finite time interval. During that time interval the velocity of the recoil changes in magnitude and direction, leading to a continuous $\gamma$-ray spectrum. If the slowing-down time is comparable to the lifetime of the level, the line shape of the observed stopped component is affected, and as a result the determined lifetime is underestimated. To account for that, a Monte Carlo simulation of the experiment, mainly of the slowing-down processes in the target and in the stopper, was carried out. The procedure is described in detail in Ref. [24]. As a result, the corrected mean lifetime for the case of $6_1^+$ was found to be 2.0(1) ps, and it is shown in Fig. 6.

#### 4. $I^\pi = 8_1^+$ state at $E_x = 3013$ keV

Lifetimes for the $8_1^+$ state were determined by one set of direct gates and one set of indirect gates. The direct gates were placed on the Doppler-shifted components of the 980-keV, $10_1^+ \rightarrow 8_1^+$ transition in rings 1 and 5. For these direct gates on the 980-keV transition, lifetimes of 1.91(11), 1.67(10), and 1.89(11) ps were observed for the 0_1, 0_5, and 6_5 ring combinations, respectively. The indirect gates were placed on the Doppler-shifted component of the 1062-keV, $12_1^+ \rightarrow 10_1^+$ transition in rings 5 and 6, which were summed as described for the $4_1^+$ and $6_1^+$ analyses. For these indirect gates, a lifetime of 1.66(20) ps was observed for the 0_5,6 ring combination. Coincidence decay curves and the resulting $\tau$ plot for the 0_5,6 ring combination are shown in Figs. 5(g) and 5(h). The weighted mean of these five lifetimes of the $8_1^+$ state is 1.80(14) ps.

As in the case of $6_1^+$, the correction described in the previous paragraph was also performed for the $8_1^+$ lifetime. The resulting mean lifetime for the $8_1^+$ after the correction is 1.9(2) ps and it is also shown in Fig. 6.

As already mentioned, Ayangeakaa *et al.* [14] measured the lifetimes of high-spin and medium-spin states in $^{102}$Pd using the Doppler-shift attenuation method. The lifetimes given therein for the $6^+$ and $8^+$ states are 1.149(32) and 0.720(42) ps, respectively, thus being significantly lower than our corresponding ones. However, we estimate that the sensitivity of the Doppler-shift attenuation method in this case is rather low since the effective lifetimes of the $6_1^+$ and $8_1^+$ states, which include the feeding times from higher-lying states, are large compared to the stopping time for the experimental setup used in [14]. The real reason for this discrepancy is unclear, however, due to the good agreement of our results with the pre-existing data for the $2^+$ and $4^+$ states as well as the better sensitivity of the Recoil Distance Doppler Shift (RDDS) method for lifetimes above 1 ps, we trust our results.

### B. Sideband lifetimes

Lifetimes of the $8_1^-$, $9_1^-$, and $10_1^-$ excited states within the higher-lying negative-parity bands were also determined in this experiment and are briefly presented in the following paragraphs. Due to lower statistics in these sideband transitions, it was necessary to gate on multiple rings and then add the cuts to yield one summed spectrum with more statistics. Hence, the cuts 0_0, 0_1, 0_5, and 0_6 were added to produce the 0_s summed spectrum. Likewise, this was performed for the other ring cuts to yield the 1_s, 5_s, and 6_s summed spectra. Using the same procedures employed for the yrast band transitions, the resulting coincidence decay curves and $\tau$ plots for the sideband transitions are shown in Fig. 7, and the weighted mean lifetimes with their corresponding errors from all ring combinations in Fig. 8.

#### 1. $I^\pi = 8_1^-$ state at $E_x = 3671$ keV

Lifetimes of the $8_1^-$ state were determined by one set of direct gates that were placed on the Doppler-shifted components of the 756-keV, $10_1^- \rightarrow 8_1^-$ transition in rings 0, 1, 5, and 6. The summed cuts of the 647-keV, $8_1^- \rightarrow 6_1^-$ transition were analyzed and yielded lifetimes of 11.9(6), 12.3(7), 11.2(6), and 12.2(7) ps for rings 0, 1, 5, and 6. The resulting coincidence decay curves and $\tau$ plot for the 0_s cut are shown in Figs. 7(a) and 7(b), and the corresponding weighted mean lifetime of 11.9(5) ps is shown in Fig. 8(a).

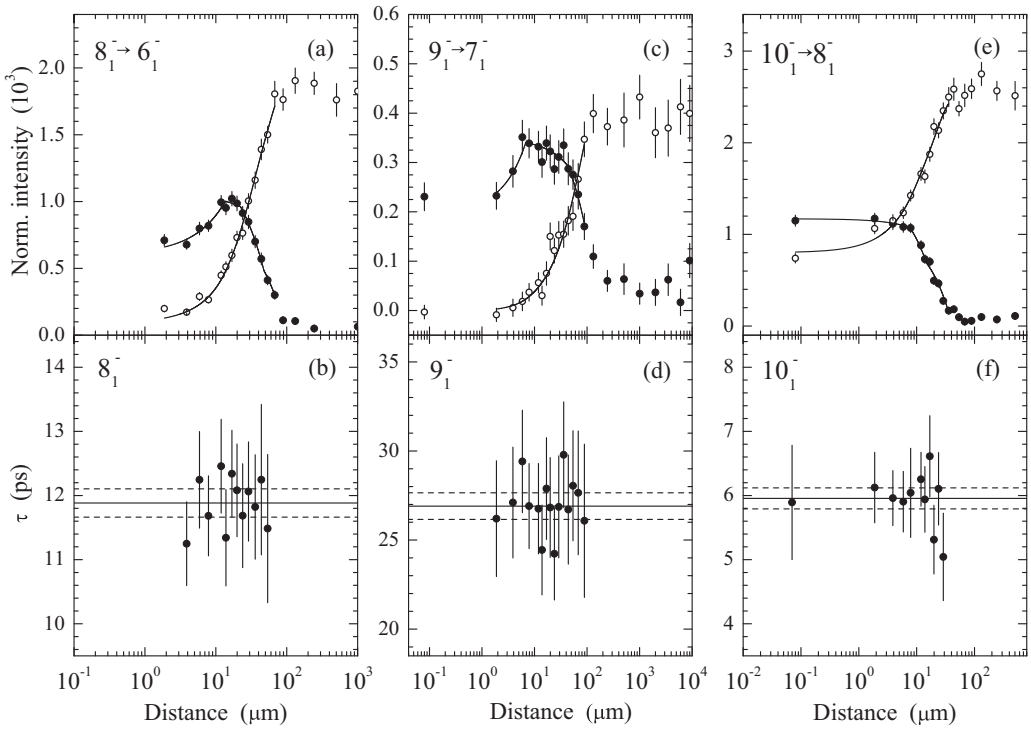


FIG. 7. Typical coincidence decay curves and $\tau$ plots for the $8_1^-$, $9_1^-$, and $10_1^-$ negative-parity sideband members are presented in (a) and (b), (c) and (d), and (e) and (f), respectively. Symbols are identical to those used in Fig. 5.

### 2. $I^\pi = 9_1^-$ state at $E_x = 3728$ keV

Lifetimes of the $9_1^-$ state were determined by one set of direct gates that were placed on the Doppler-shifted components of the 705-keV, $11_1^- \rightarrow 9_1^-$ transition in rings 0, 1, 5, and 6. The summed cuts of the 540-keV, $9_1^- \rightarrow 7_1^-$ transition were analyzed and yielded lifetimes of 27.1(16), 26.1(16), 26.9(16), and 28.1(16) ps for rings 0, 1, 5, and 6. The resulting coincidence decay curves and $\tau$ plot for the 5_s cut are shown in Figs. 7(c) and 7(d), and the corresponding weighted mean lifetime of 27.1(8) ps is shown in Fig. 8(b).

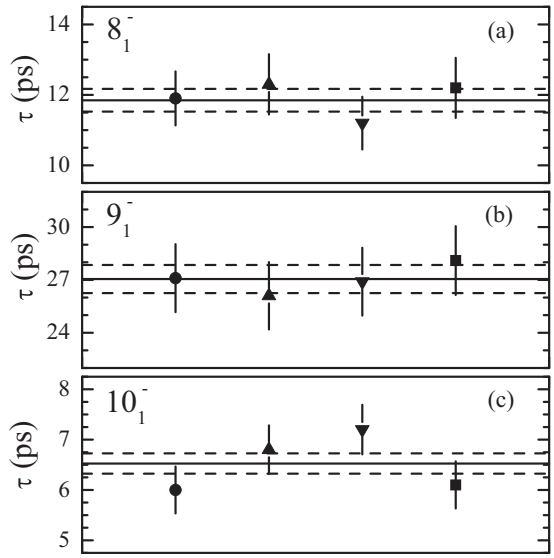


FIG. 8. Compilation of the weighted mean lifetimes of the negative-parity sideband levels (a) $8_1^-$, (b) $9_1^-$, and (c) $10_1^-$ deduced in this work and their associated errors. In all cases direct gating was used. Circles, upward triangles, downward triangles, and squares correspond to projection rings 0, 1, 5, and 6, respectively. As in the case of yrast lifetimes, to determine the total uncertainty of those weighted mean lifetimes the average weighted variance was taken. Solid and dashed lines, which represent the weighted mean values and their associated errors, are listed in Table I.

### 3. $I^\pi = 10_1^-$ state at $E_x = 4318$ keV

Lifetimes of the $10_1^-$ state were determined by one set of direct gates that were placed on the Doppler-shifted components of the 776-keV, $12_1^- \rightarrow 10_1^-$ transition in rings 0, 1, 5, and 6. The summed cuts of the 647-keV, $10_1^- \rightarrow 8_1^-$ transition were analyzed and yielded lifetimes of 6.0(4), 6.8(4), 7.2(4), and 6.1(4) ps for rings 0, 1, 5, and 6. The resulting coincidence decay curves and $\tau$ plot for the 0_s cut are shown in Figs. 7(e) and 7(f), and the corresponding weighted mean lifetime of 6.5(6) ps is shown in Fig. 8(c).

## IV. DISCUSSION

It has been suggested in the past, in [12] and [13], that $^{102}$Pd is a good candidate for the E(5) critical-point symmetry. This assumption was mainly based on the $R_{4/2}$ ratio, the normalized $B(E2; 4_1^+ \rightarrow 2_1^+)$ and $B(E2; 4_2^+ \rightarrow 2_2^+)$ transition strengths, and the reasonable agreement of the $0_3^+$ properties when it is identified as the $0_\xi^+$ of the E(5) picture.

However, striking discrepancies from the expected values have been stressed in both references. Namely, the normalized $B(E2; 2_2^+ \rightarrow 2_1^+)$ value is more than a factor of 3 lower than expected and the $B(E2; 4_2^+ \rightarrow 4_1^+)$ has an upper limit which

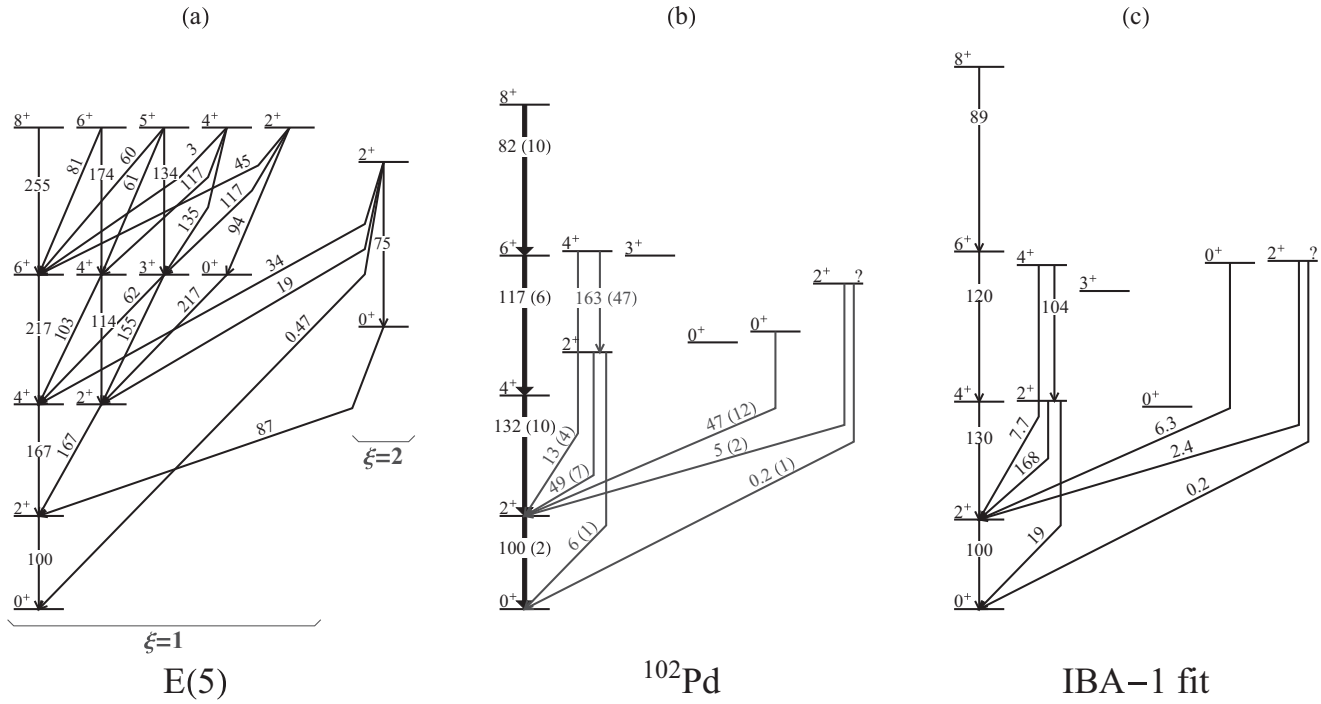


FIG. 9. Complete up-to-date level scheme of $^{102}$Pd is shown in (b) next to the E(5) critical-point symmetry level scheme (a) and an IBA-1 fit (c). Transition strengths are normalized on the $B(E2;2_1^+ \to 0_1^+)$ value. In (b), the strengths of the yrast transitions (bold black arrows) are derived in this work, whereas the rest are taken from the most recent compilation of evaluated data for $A = 102$ [29]. E(5) excitation energies and transition strengths are taken from [27]. The comparison is clearly does not favor the characterization of $^{102}$Pd as an E(5) nucleus. In addition, a general IBA-1 Hamiltonian was necessary in order to describe the yrast transition strengths well, which also contradicts the E(5) hypothesis.

is a factor of 2 too low. Moreover, the energy and lifetime of the $0_2^+$ cannot fit in the E(5) model space as the member of the three-phonon multiplet. This has led to its characterization as an intruder state, thus leaving a vacant candidacy for the role of $0_\tau^+$ in the E(5) picture.

This work clears up the situation, as it complements the literature with the transition strengths for the yrast band up to the $8_1^+$ level (see Table I). The normalized transitions strengths derived in this work along with the existing literature values are shown in Fig. 9 next to the E(5) level scheme. The $B(E2;2_1^+ \to 0_1^+)$ value determined in this work is in very good agreement with the adopted value [25]. $B(E2;4_1^+ \to 2_1^+)$ is significantly smaller than the previously measured value in [26] and deviates from the E(5) prediction. To complete the picture, as shown in Fig. 9, the decreasing $B(E2;6_1^+ \to 4_1^+)$ and $B(E2;8_1^+ \to 6_1^+)$ transition strengths come in clear disagreement with the increasing trend predicted by the E(5) critical-point symmetry.

Also, in view of the new data given in this work for the yrast transitions, an IBA-1 fit was made, which is also shown in Fig. 9(c). The fit was made using the IBA-1 code of Van Isacker [28]. Initially, the IBA Hamiltonian used was

$$H = \epsilon \hat{n}_d + \alpha_0 \hat{P}^\dagger \cdot \hat{P} + \alpha_3 \hat{T}_3 \cdot \hat{T}_3, \tag{4}$$

which describes the transition between U(5) and O(6), as proposed in [12]. It soon became obvious that in order to describe the yrast $B(E2)$'s well up to $8_1^+$, more terms must be included. In particular, the Hamiltonian used for the IBA-1 fit shown in Fig. 9 is

$$H = \epsilon \hat{n}_d + \alpha_0 \hat{P}^\dagger \cdot \hat{P} + \alpha_1 \hat{L} \cdot \hat{L} + \alpha_2 \hat{Q}_\chi \cdot \hat{Q}_\chi + \alpha_3 \hat{T}_3 \cdot \hat{T}_3, \tag{5}$$

where the parameters used for the fit were $\epsilon = 0.68$ MeV, $\alpha_0 = 0.2$ MeV, $\alpha_1 = 0.015$ MeV, $\alpha_2 = 0.025$ MeV, and $\alpha_3 = 0.050$ MeV. The $E2$ transitions are described by the operator

$$T(E2) = e_2[s^\dagger \tilde{d} + d^\dagger s + \chi(d^\dagger \tilde{d})^{(2)}], \tag{6}$$

where the boson effective charge was taken as $e_2 = 0.1266e \cdot b$ and the parameter $\chi$ was taken equal to $-\sqrt{7}/2$ in both the $\hat{Q}_\chi$ operator of the Hamiltonian and the $T(E2)$ operator in order to lie within the consistent $q$ formalism. The fact that an IBA-1 Hamiltonian more general than the one proposed in [12] is needed to describe the data [12] is also a good indication that $^{102}$Pd cannot be described in terms of the $E(5)$ critical-point symmetry.

In order to further investigate the structure of $^{102}$Pd, the parameters of the fit were used to calculate the energy functional of the Hamiltonian in the geometrical limit of the IBM [30]; that is,

$$E(\beta,\gamma) = \frac{N}{1+\beta^2}(0.125 + 0.909\beta^2) + \frac{N(N-1)}{(1+\beta^2)^2} \times (0.063\beta^4 + 0.071\beta^3 \cos(3\gamma) + 0.05), \tag{7}$$

where $N = 5$ is the boson number. In Fig. 10 the contours of this energy functional are plotted in the $\beta, \gamma$ plane. As shown in this plot the nucleus appears to be quite $\gamma$-soft, with a tendency

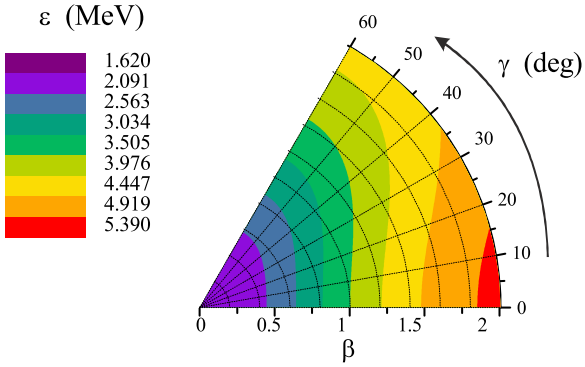


FIG. 10. Contours of the energy functional for the case of $^{102}$Pd in the $\beta$, $\gamma$ plane as obtained in our IBM-1 fit. The fact that the potential surfaces are not concentric shows that the nucleus is not spherical but, rather, characterized by some degree of triaxiality, favoring lower deformations $\beta$ on the prolate side ($\gamma = 0^\circ$) and larger ones on the oblate side ($\gamma = 60^\circ$).

for larger values of $\beta$ for larger $\gamma$'s. Although not very far from sphericality, the potential appears to have prolate-oblate shape differences, which show signs of deformation and thus deviations from the U(5) limit where the potential is expected to be symmetric in $\gamma$.

In an attempt to test the proximity of the structure of $^{102}$Pd to that of an O(6) nucleus, the ground state of $^{102}$Pd, as obtained from our IBM calculation, was represented in an O(6) basis for five bosons. The resulting expansion is

$$\begin{aligned}|0_1(^{102}\mathrm{Pd})\rangle = &-0.7198|0_1^+\mathrm{O}(6)\rangle + 0.0590|0_2^+\mathrm{O}(6)\rangle \\ &+ 0.6293|0_3^+\mathrm{O}(6)\rangle - 0.0121|0_4^+\mathrm{O}(6)\rangle \\ &+ 0.2867|0_5^+\mathrm{O}(6), \end{aligned} \quad (8)$$

where $|0_i^+\mathrm{O}(6)\rangle$ is the $i$th $0^+$ state in the O(6) limit for $N = 5$. If $^{102}$Pd were close to the O(6) limit, one would expect to obtain an expansion which would be strongly governed by the first term, which corresponds to the ground state of an O(6) nucleus. Instead, there is a strong mixing of the first and third $0^+$ states of the O(6) basis, which correspond to different values of the quantum number $\sigma$. The latter shows that $^{102}$Pd is rather far from the O(6) limit, as there is a mixing of states of different structures.

On the other hand, as shown below, the same expansion on an U(5) basis shows that the ground state in our IBM-1 calculation is nearly purely U(5) (93.5%):

$$\begin{aligned}|0_1(^{102}\mathrm{Pd})\rangle = &\ 0.9671|0_1^+\mathrm{U}(5)\rangle + 0.2275|0_2^+\mathrm{U}(5)\rangle \\ &+ 0.1133|0_3^+\mathrm{U}(5)\rangle + 0.0133|0_4^+\mathrm{U}(5)\rangle \\ &- 0.0056|0_5^+\mathrm{U}(5). \end{aligned} \quad (9)$$

However, the second and third $0^+$ states are strongly mixed:

$$\begin{aligned}|0_2(^{102}\mathrm{Pd})\rangle = &\ 0.2458|0_1^+\mathrm{U}(5)\rangle - 0.7201|0_2^+\mathrm{U}(5)\rangle \\ &- 0.6341|0_3^+\mathrm{U}(5)\rangle - 0.1210|0_4^+\mathrm{U}(5)\rangle \\ &+ 0.0652|0_5^+\mathrm{U}(5), \end{aligned} \quad (10)$$

$$\begin{aligned}|0_3(^{102}\mathrm{Pd})\rangle = &\ 0.0600|0_1^+\mathrm{U}(5)\rangle - 0.6258|0_2^+\mathrm{U}(5)\rangle \\ &+ 0.7617|0_3^+\mathrm{U}(5)\rangle - 0.1553|0_4^+\mathrm{U}(5)\rangle \\ &- 0.0183|0_5^+\mathrm{U}(5). \end{aligned} \quad (11)$$

The same feature is observed for other spins too, which points to the fact that in the transitional nucleus $^{102}$Pd the structure of the states changes with the excitation energy. This may also explain the deviations in the yrast $B(E2)$ values from the U(5) expectations. It is thus concluded that $^{102}$Pd is rather far from the O(6) limit and, to a lesser extent, from the U(5) one.

Finally, according to our IBA-1 calculation, the mean value of the deformation parameter $\gamma$ is calculated as 31.3°, 42.8°, and 15.4° for the $0_1^+$, $0_2^+$, and $0_3^+$ states, respectively. Therefore, the coexistence of states with different shapes is predicted for this transitional nucleus.

## V. CONCLUSIONS

Lifetimes of yrast and nonyrast states of $^{102}$Pd have been measured through a Recoil Distance Doppler Shift (RDDS) measurement. The derived $B(E2)$ values for yrast transitions up to the $8_1^+$ level were compared with the predictions of the E(5) critical-point symmetry, showing a clear disagreement. Thereby, one of the few proposed candidates for the E(5) symmetry has been ruled out, leaving $^{134}$Ba as the only current candidate.

## ACKNOWLEDGMENTS

This work was supported in part by the FP7/REGPOT/LIBRA project (Grant No. 230123) and the German Research Foundation (DFG) under Contract No. DE1516/3-1. P.P. is grateful for the financial support from the Bulgarian Science Fund under Contract DFNI-E 01/2.

[1] F. Iachello, Phys. Rev. Lett. **85**, 3580 (2000).
[2] F. Iachello, Phys. Rev. Lett. **87**, 052502 (2001).
[3] A. Bohr, Mat.-Fys. Medd. Danske Vid. Selsk. **26**(14) (1952).
[4] G. Scharff-Goldhaber and J. Weneser, Phys. Rev. **98**, 212 (1955).
[5] L. Wilets and M. Jean, Phys. Rev. **102**, 788 (1956).
[6] A. Arima and F. Iachello, Ann. Phys. **99**, 253 (1976); **111**, 201 (1978); **123**, 468 (1979).
[7] R. F. Casten and N. V. Zamfir, Phys. Rev. Lett. **87**, 052503 (2001).
[8] R. Krücken, B. Albanna, C. Bialik, R. F. Casten, J. R. Cooper, A. Dewald, N. V. Zamfir, C. J. Barton, C. W. Beausang, M. A. Caprio, A. A. Hecht, T. Klug, J. R. Novak, N. Pietralla, and P. von Brentano, Phys. Rev. Lett. **88**, 232501 (2002).
[9] D. Tonev, A. Dewald, T. Klug, P. Petkov, J. Jolie, A. Fitzler, O. Möller, S. Heinze, P. von Brentano, and R. F. Casten, Phys. Rev. C **69**, 034334 (2004).
[10] A. Dewald, O. Möller, B. Saha, K. Jessen, A. Fitzler, B. Melon, T. Pissulla, S. Heinze, J. Jolie, K. O. Zell, P. von Brentano, P. Petkov, S. Harissopulos, G. De Angelis, T. Martinez, D. R. Napoli, N. Marginean, M. Axiotis, C. Rusu, D. Tonev, A. Gadea, Y. H. Zhang, D. Bazzacco, S. Lunardi, C. A. Ur, R. Menegazzo, and E. Farnea, J. Phys. G: Nucl. Part. Phys. **31**, S1427 (2005).

[11] R. F. Casten and N. V. Zamfir, Phys. Rev. Lett. **85**, 3584 (2000).
[12] N. V. Zamfir, M. A. Caprio, R. F. Casten, C. J. Barton, C. W. Beausang, Z. Berant, D. S. Brenner, W. T. Chou, J. R. Cooper, A. A. Hecht, R. Krücken, H. Newman, J. R. Novak, N. Pietralla, A. Wolf, and K. E. Zyromski, Phys. Rev. C **65**, 044325 (2002).
[13] R. M. Clark, M. Cromaz, M. A. Deleplanque, M. Descovich, R. M. Diamond, P. Fallon, I. Y. Lee, A. O. Macchiavelli, H. Mahmud, E. Rodriguez-Vieitez, F. S. Stephens, and D. Ward, Phys. Rev. C **69**, 064322 (2004).
[14] A. D. Ayangeakaa, U. Garg, M. A. Caprio, M. P. Carpenter, S. S. Ghugre, R. V. F. Janssens, F. G. Kondev, J. T. Matta, S. Mukhopadhyay, D. Patel, D. Seweryniak, J. Sun, S. Zhu, and S. Frauendorf, Phys. Rev. Lett. **110**, 102501 (2013).
[15] T. K. Alexander and J. S. Forster, in *Advances in Nuclear Physics*, edited by M. Baranger and E. Vogt (Plenum Press, New York, 1978), Vol. 10, p. 197.
[16] A. Dewald, O. Möller, and P. Petkov, Prog. Particle Nucl. Phys. **67**, 786 (2012).
[17] C. Rossi Alvarez, Nucl. Phys. News **3**, 10 (1993).
[18] A. Dewald, S. Harissopulos, and P. von Brentano, Z. Phys. A. **334**, 163 (1989).
[19] G. Böhm, A. Dewald, P. Petkov, and P. von Brentano, Nucl. Instrum. Methods Phys. Res. A **329**, 248 (1993).
[20] B. Saha, NAPATAU (Institute of Nuclear Physics, Cologne, unpublished).
[21] J. Theuerkauf, S. Esser, S. Krink, M. Luig, N. Nicolay, O. Stuch, and H. Wolters, TV (Institute of Nuclear Physics, Cologne, unpublished).
[22] R. Rascher, K. P. Lieb, and M. Uhrmacher, Phys. Rev. C **13**, 1217 (1976).
[23] P. Petkov, Nucl. Instrum. Methods Phys. Res. A **349**, 289 (1994).
[24] P. Petkov, D. Tonev, J. Gableske, A. Dewald, T. Klemme, and P. von Brentano, Nucl. Instrum. Methods Phys. Res. A **431**, 208 (1999).
[25] J. Lange, A. T. Kandil, J. Neuber, C. D. Uhlhorn, and H. Von Buttlar, Nucl. Phys. A **292**, 301 (1977).
[26] M. Luontama, R. Julin, J. Kantele, A. Passoja, W. Trzaska, A. Bäcklin, N. G. Jonsson and L. Westerberg, Z. Phys. A. **324**, 317 (1986).
[27] M. A. Caprio and F. Iachello, Nucl. Phys. A **781**, 26 (2007).
[28] P. Van Isacker (private communication).
[29] D. De Frenne, Nucl. Data Sheets **110**, 1745 (2009).
[30] P. Van Isacker and J. Q. Chen, Phys. Rev. C **24**, 684 (1981).